International Journal of Concrete Structures and Materials

RESEARCH Open Access

Experimental Investigations on Tensile and Shear Behavior of the Interface Between UHP-ECC and Concrete

Jun-Jie Zeng[1,2], Xin-Chao Lin[1], Sheng-Zhao Feng[1], Jiong-Yi Zhu[3*], Yan Zhuge[2] and Yihang Yan[4]

Abstract

Ultra-high performance engineered cementitious composite (UHP-ECC), which is known for its exceptional compressive strength, tensile strength, and ductility, has been emerged as a promising option for repairing and strengthening reinforced concrete (RC) structures. The bond between UHP-ECC and normal concrete is the key issue for the material to be successfully implemented. This paper presents an experimental investigation focused on understanding the tensile and shear behavior of the bonding interface between UHP-ECC and concrete. A total of 78 specimens were prepared and tensile splitting tests and push-out tests were carried out. The study examined key parameters including the strength of the concrete substrate, the roughness of the interface, and the moisture condition at the interface. Various failure modes are observed in the specimens under tensile splitting force and direct shear force, and it is found that the influence of the key parameters varied depending on the type of failure mode. In specimens experiencing full interface debonding or interface failure combined with substrate cracks, the roughness of the interface and the moisture degree have a significant impact on the tensile and shear strength. Conversely, in specimens with full substrate disruption, the strength of the substrates plays a more significant role. Additionally, the study reveals that the grooving treatment is highly effective in improving the shear strength of the interface, but its impact on enhancing the tensile strength is comparatively less pronounced. Prediction models for the tensile and shear strength of the interface are established and verified against the test results. The proposed models provide valuable insights into the behavior of the UHP-ECC to concrete interface and can aid in predicting its performance in practical applications.

Keywords UHP-ECC, Interfacial bonding, Splitting tensile test, Push-out test, Repair material

1 Introduction

Structural strengthening has become increasingly necessary due to a range of factors. One significant factor is the aging of buildings and infrastructure worldwide. Many existing structures do not meet current design codes and standards, making strengthening essential to ensure they can withstand anticipated loads and maintain their structural integrity. Over time, structural strengthening techniques have progressed due to advancements in construction materials, engineering expertise, and technology. This progress has led to the development of various materials that are now accessible to cater to specific strengthening needs (Li, 2003; Yoo & Banthia, 2016; Yu

Journal information: ISSN 1976-0485 / eISSN 2234-1315.

*Correspondence:
Jiong-Yi Zhu
shuzhujy@shu.edu.cn
[1] Department of Civil Engineering, Guangdong University of Technology, Guangzhou 510006, China
[2] UniSA STEM, University of South Australia, South Australia 5095, Australia
[3] Department of Civil Engineering, School of Mechanics and Engineering Science, Shanghai University, Shanghai, China
[4] Shanghai Urban Construction and Design Research Institute (Group) Co., Ltd, Shanghai Engineering Technology Research Center of Industrialized and Prefabricated Municipal Civil Engineering, Shanghai 200444, China

et al., 2018). Engineered Cementitious Composite (ECC) is an advanced construction material that has gained considerable attention in recent years for its exceptional tensile strength, ductility and durability which are potential for structural strengthening applications (Ding et al., 2018; Li, 2003; Li et al., 2001). The interaction between the fibers and matrix in ECC is modified to achieve strain-hardening behavior and features multiple instances of micro-cracking with self-controlled widths (Yu et al., 2018). Ultra-high performance concrete (UHPC) is another advanced material known for its exceptional compressive strength, making it a preferred choice for use in compressive members (Wang et al., 2023b; Zhao et al., 2023). In recent years, significant research and development have focused on ultra-high performance engineered cementitious composites (UHP-ECC). By incorporating polyethylene (PE) fibers and utilizing a low water/binder ratio, ECC has achieved remarkable tensile strengths exceeding 10 MPa and elongations exceeding 5% while an impressive compressive strength exceeding 100 MPa also have been attained (Li et al., 2019; Yu et al., 2018, 2020). The exceptional strength and ductility of UHP-ECC materials offer substantial benefits to structures subjected to extreme loads like earthquakes, as they can absorb a substantial amount of energy. ECC has garnered significant research attention as an exceptional material for structural strengthening, prompting extensive research into its strengthening capabilities. It has been demonstrated that ECC as well as fiber-reinforced polymer (FRP) reinforced ECC hold tremendous potential for strengthening RC columns (Li et al., 2023; Zeng et al., 2023; Zhang et al., 2019, 2021; Zeng et al. 2024; Yan et al. 2024; Lin etal. 2024), masonry walls (Deng et al., 2019; Lin et al., 2014; Yu et al., 2022) and RC beams (Li et al., 2021; Tian et al., 2022; Yang et al., 2018; Ye et al., 2023). Various studies have emphasized the crucial role of interfacial bonding behavior between the additive material and the existing concrete in determining the effectiveness of repairs or strengthening (El Afandi et al., 2023; Pan et al., 2022) because the effectiveness of bonding notably secure jointly action of both the strengthening material and the existing concrete.

Extensive experimental studies have been conducted to investigate the bonding behavior between repairing materials and substrate concrete, highlighting the importance of various factors. These factors include substrate surface roughness (Júlio et al., 2004; Santos et al., 2007; Wang et al., 2018, 2023a; Zhang et al., 2023), strength and stiffness differences between new and old materials (Tian et al., 2019; Zhang et al., 2020), shrinkage(Farzad et al., 2019; Zhang et al., 2020), moisture conditions (Luo et al., 2023; Zhang et al., 2020) and the presence of fibers (Ju et al., 2020; Qasim et al., 2022; Zanotti et al., 2017). Consensus has been reached among existing studies that substrate surface roughness is a critical parameter affecting the bonding strength of the interface. Surface roughness treatment has been shown to significantly enhance the interfacial bonding between the substrate and the repairing material. For instance, Zhang et al. (2023) investigated the impact of surface roughness on the bonding behavior of the UHP-ECC to old concrete interface, observing a substantial improvement in shear strength and a moderate post-peak shear degradation due to the roughness treatment. Similar observations have also been made in studies examining the tensile and shear behavior of the interface between UHPC and concrete (Zhang et al., 2020). The strength and stiffness difference between the repairing material and the substrate also play a crucial role in the bonding behavior (Diab et al., 2017; Tian et al., 2019). Research has shown that a significant difference in strength and stiffness can lead to stress concentration at the interface edge, resulting in premature failure (Diab et al., 2017). However, Tian et al. (2019) observed that the strength grades of ECC had no influence on the failure mode and shear behavior of the ECC-concrete interface. Moisture conditions at the interface have also been found to influence the bonding behavior (Bentz et al., 2018; Luo et al., 2023; Semendary & Svecova, 2020; Zhang et al., 2020). Zhang et al. (2020) discovered that specimens with a saturated surface dry condition achieved higher bonding capacity compared to those with an air surface dry condition. However, different conclusions have been drawn from other studies (Luo et al., 2023; Semendary & Svecova, 2020), where test results indicated that the surface moisture condition only reduced the variability of failure mode and shear capacity but had a minor influence on the ultimate strength value. Bentz et al. (2018) suggested that under air dry surface conditions, the dry surface absorbs water from the fresh repairing material, leading to condensation of particles at the interface. They found that these condensed particles improved bonding performance under slant shear tests but had no impact on tensile stresses. The effect of fiber types and volume fraction on the interfacial bonding behavior has also been investigated (Ju et al., 2020; Qasim et al., 2022; Zanotti et al., 2014). The experimental results from Zanotti et al. (2014) demonstrate that the inclusion of Polyvinyl Alcohol (PVA) fibers significantly enhances the cohesion at the bond interface, improving the overall bonding behavior. Additionally, Qasim et al. (2022) discovered that in interfaces treated with sandblasting, the presence of steel fibers establishes a dowel action that further enhances the interfacial bonding. Furthermore, Ju et al. (2020) observed that increasing the volume fraction of fibers can effectively enhance the splitting tensile strength of the bonding interface.

Table 1 Concrete mix proportions (Unit: kg)

Series	Cement	Fly ash	Mineral powder	Coarse aggregate	Quartz powder	Silica fume	River Sand	Water	Superplasticizer	PE fiber
UHP-ECC	1	N.A	0.94	N.A	0.63	0.19	N.A	0.33	0.05	1%
HSC	1	N.A	N.A	1.77	N.A	N.A	1.30	0.32	0.01	N.A
NSC	1	0.27	0.20	4.19	N.A	N.A	2.67	0.67	0.038	N.A

1%—Fiber volume fraction of 1.0%, *N.A.* not applicable

Table 2 Compressive properties of the concrete and UHP-ECC

Series	Peak strength f_{co}′(MPa)	Elastic modulus E_c (GPa)	Peak strain ε_{co} (%)
UHP-ECC	108.3	35.2	0.32
HSC	74.4	33.9	0.26
NSC	50.0	31.9	0.23

Table 3 Tensile properties of the UHP-ECC

Specimens	Initial cracking stress σ_{tc}(MPa)	Peak stress σ_{pc} (MPa)	Peak strain ε_{pc} (%)
UHP-ECC-1	6.4	10.4	4.5
UHP-ECC-2	6.4	11.7	5.4
UHP-ECC-3	6.3	12.2	4.4
Avg	6.4	11.4	4.8

The current body of literature indicates that the bonding behavior between new repairing materials and the substrate concrete is influenced by a multitude of factors. However, the precise impact of these factors remains unclear, particularly when it comes to newly developed high-performance materials such as UHP-ECC. To this end, this paper presents an experimental investigation aimed at examining the impact of key parameters on the tensile and shear behavior of the interface between UHP-ECC and concrete.

2 Experimental Program

2.1 Material

The mix proportions of the concrete substrates and repair material UHP-ECC are listed in Table 1. The UHP-ECC is composited of Portland cement (P•O 52.5R), silica sand with a particle size ranged from 0.076 to 0.150 mm, silica fume with a particle size ranged from 0.1 to 1 μm and polyethylene (PE) fibers with a length of 18 mm. The compressive properties of the material were achieved based on the specified compressive test method in accordance with ASTM C469-2014 (ASTM, 2014), and the results are listed in Table 2. The compressive properties of UHP-ECC were achieved from compressive tests on three Φ50 × 150 mm cylinders. The ultimate compressive strength and elastic modulus are 108.3 MPa and 35.2 GPa respectively. Two grades of concrete substrates are adopted in the experiment. The compressive strength of normal strength concrete (NSC) and high strength concrete (HSC) was obtained from compressive tests on standard concrete cylinders with a diameter of 150 mm and height of 300 mm, two strain gauges were attached onto the cylinders to achieve the elastic modulus of concrete. The compressive strength and elastic modulus of the NSC are 50.0 MPa and 31.9 GPa respectively, and the compressive strength and elastic modulus of the HSC are 74.4 MPa and 33.9 GPa. The tensile properties of UHP-ECC are collected from tensile coupon tests with three dog-bone-shaped UHP-ECC coupons. The averaged initial cracking stress, peak tensile stress, and peak tensile strain are 6.4 MPa, 11.4 MPa, and 4.8% respectively as shown in (Table 3).

2.2 Test Methods and Specimens

Various test methods have been employed to study the interfacial bonding behavior between repair materials and substrate concrete. The objective of this study is to examine the tensile and shear behavior of the UHP-ECC to concrete interface. To achieve this, splitting tensile tests and double-sided direct shear tests were conducted. In the splitting tensile test, a compressive load was applied along the longitudinal direction of the interface to generate a splitting tensile force between the substrate and the repair material. The loading rate used in these tests was set at 0.2 mm/min to ensure accurate and reliable results. The test setup of the splitting tensile test is shown in Fig. 1a. The push-out test, a type of direct shear test with a double-sided interface, was employed to accurately measure the pure shear capacity of the interface. Unlike the common direct shear test with a single interface, the double-sided direct shear test offers improved safety and stability due to the symmetric shear load applied. The test setup for the push-out tests is illustrated in Fig. 1b. To analyze the stress distribution near the interface and record the failure progression of the specimens, the Digital Image Correlation (DIC) technique was

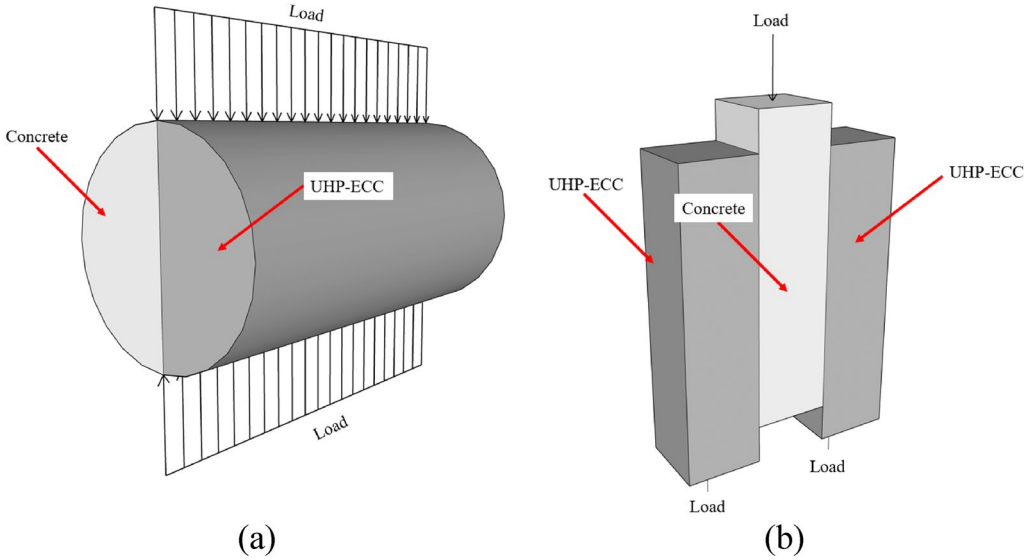

Fig. 1 Test setup: **a** Splitting tensile test and **b** Push-out test

utilized. The loading rate for the push-out tests was set at 0.2 mm/min to ensure reliable and precise results.

2.3 Preparation of Specimens

The composite cylinder specimen with Φ100 × 200 mm dimensions was prepared for splitting tensile tests. The procedures for splitting tensile specimens are shown in Fig. 2. Firstly, PVC tubes and half-section polystyrene foams were used to build the formworks for substrate concrete. To attain the grooved interface, the polystyrene foams were shaped with desired grooves. After the formworks are ready, concrete substrates were cast and demolded after 24 h, and then cured in a laboratory environment for 28 days. Then, surface treatments were conducted on the concrete substrate surface. Existing studies have the agreement that substrate surface roughness plays a fundamental role in the interface bonding strength, thus the surface roughness is the major parameter have been studied in this work. The sand-patch method specified in ASTM E965 (ASTM, 2019) was used to evaluate the surface roughness of the substrate due to its simplicity and convenient operation. Three levels of surface roughness with average macrotexture depths of 0.4 mm, 0.8 mm, and 1.2 mm were studied in the experimental program, in addition, substrate surfaces with grooves were also prepared and investigated. The influence of moisture degree at the surface of the substrate on the interface behavior was also investigated. Two types of surface conditions were considered, the first one is the air surface dry condition (ASD), in which the surface of the concrete substrate was placed in a dry environment for at least 7 days before casting of UHP-ECC. Another condition was the saturated surface dry condition (SSD), in which the concrete substrates were cured in the water tank for at least 48 h before casting. After the surface treatments were done, UHP-ECC half was cast against the concrete substrate, and finally, the specimens were demoulded after 24 h and cured for more than 28 days.

For the push-out test, the specimens were cast in three portions, the middle portion is a concrete prism with a 50 mm × 50 mm square section and 200 mm height, at each side of the prism, UHP-ECC prisms were cast with the same dimension, and there was a 25 mm gap in the longitudinal direction between the substrate and the repair material for load applying. Fig. 3 shows the preparation of specimens of push-out tests. The middle-portion concrete was cast first, and after the curing of the concrete, the surface treatment was conducted on the two sides of the concrete substrate prisms, after that, the UHP-ECC portions were cast and cured at room temperature for at least 28 days.

Totally 78 specimens were cast, and the main parameters investigated are the strength of concrete substrates, interface roughness and interface moisture degree. The details of the specimens could be found in Table 4. The label system for the specimens is designed as follows. The first term stands for the test method, where S is for splitting tensile tests and P is for push-out tests. The second term stands for the strength of concrete substrates, where C1 is for normal concrete with a cylinder strength of 50 MPa, and C2 is for high-strength concrete with a strength of 74.4 MPa. The third term stands for interface roughness where R0, R1, R2, R3, and R4 are for smooth surface, with macrotexture depths of 0.4 mm, 0.8 mm, 1.2

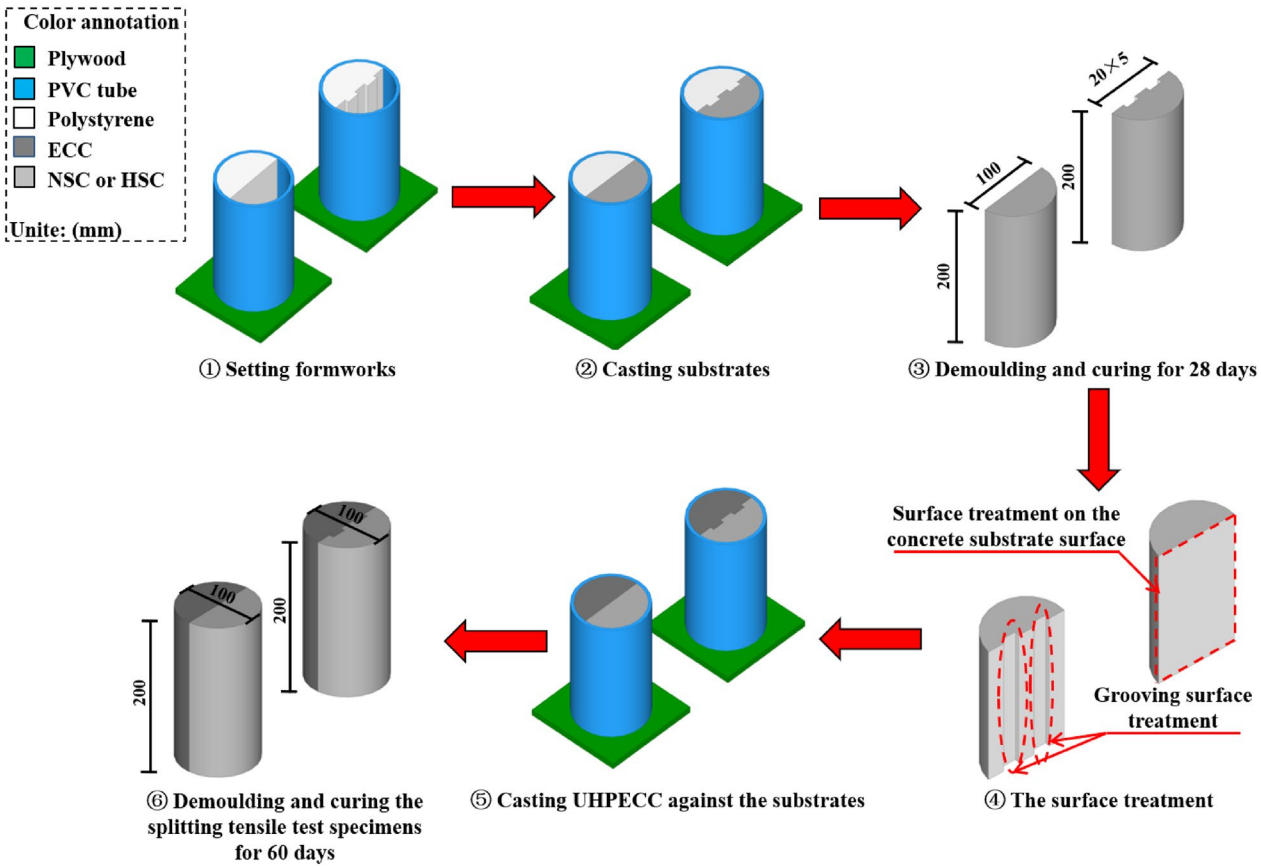

Fig. 2 Fabrication progress and dimension of the splitting tensile test specimens

mm, and grooved surface respectively. The fourth term stands for surface moisture degree, where A is for air surface dry condition, and S is for saturated surface dry condition. The final term presents the repeated specimen number. For instance, specimen label "S-C1-R0-A-1" presents the splitting tensile specimen with normal strength concrete substrate, smooth interface with air surface dry condition, and repeated specimen No. 1 (Table 4).

3 Test Results

The results of the splitting tensile tests and push-out tests are presented in Table 5. The table provides information on the ultimate strength achieved and the corresponding failure modes observed in each test. In the subsequent sections, the impact of various factors on the tensile and shear behavior of the concrete to UHP-ECC interface is discussed. The influence of surface roughness, strength disparity between the repair material and substrates, and moisture content at the interface are specifically examined. By analyzing these factors, a better understanding of the interfacial performance can be gained, leading to the development of more effective repair strategies and materials for concrete structures.

3.1 Failure Modes

Fig. 4 shows the failure patterns of splitting tensile specimens. Four types of failure modes were found. The first one is full interface failure (S-FM1), where the repair material and substrates debonded at the interface, and no cracks were found in either UHP-ECC or concrete portions. Fig. 4a shows a typical failure mode of full interface failure. The second type of failure is interface failure combined with substrate cracks (S-FM2). In such failure mode, the cracks initially formed in the concrete substrate and subsequently spread to the interface between the UHP-ECC and concrete, and continued to propagate (see Fig. 4b). The third type of failure mode is full substrate failure (S-FM3). The failure took place in the concrete substrate close to the interface, resulting in crushing or fracturing, while the UHP-ECC to concrete interface remained intact (see Fig. 4c). Specimens exhibiting failure mode S-FM3 demonstrated a significant bond between UHP-ECC and concrete, resulting in the initiation of failure due to material damage within the concrete substrate. The fourth failure mode is the bond disruption with joint torn-off (S-FM4) for the specimens with a grooved interface as shown in Fig. 4d. In all the

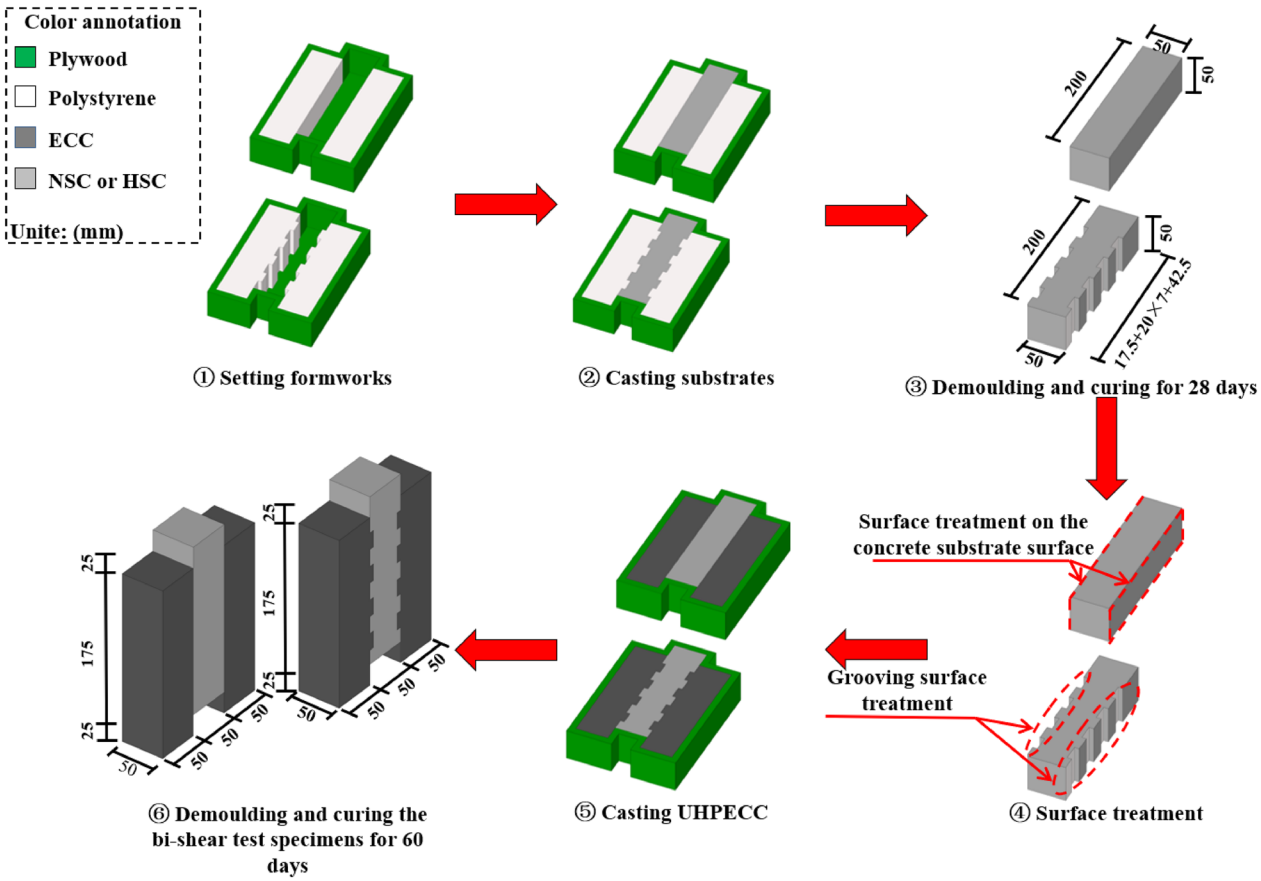

Fig. 3 Fabrication progress and dimension of the push-out test specimens

splitting tensile tests, no failure was found in the repair material UHP-ECC, due to the high tensile strength of the UHP-ECC material.

In push-out tests, three different types of failure modes were found which is shown in Fig. 5. The first one (P-FM1) is similar to the failure mode S-FM1 in the splitting tensile test, pure interface debonding was found, and either the substrate or the repair material fractured (see Fig. 5a). The second type of failure is the shear failure in concrete substrates (P-FM2), in which a major crack penetrated the concrete substrate near the interface (see Fig. 5b). The third type of failure is joint failure (P-FM3) in these specimens with grooved interfaces (see Fig. 5c).

In Table 5, the failure modes of all specimens are listed. In the splitting tensile tests, it was observed that the failure modes of the specimens were mainly influenced by the surface roughness. Pure interface failure (S-FM1) occurred in all the specimens without interface treatment. However, when the macrotexture depths of surface roughness reached 0.4, interface failure combined with substrate cracks (S-FM2) occurred. Specimens with roughness levels R2 or R3 experienced substrate failure, while all the grooved specimens had their joint keys torn off (S-FM4). In push-out tests, a similar observation was made. All specimens with a smooth interface exhibited pure interface failure (P-FM1), whereas specimens with interface macrotexture depths ranging from 0.4 to 1.2 experienced shear failure in the concrete substrates (P-FM2). Additionally, failure (P-FM3) with sheared-off joint keys was found in specimens with grooved interfaces. The DIC technology captured the history of strain distribution of the push-out test specimens. The strain distribution of specimens with P-FM1 failure mode is shown in Fig. 6a, in which interface bond disruption occurred at one side of the specimen and the load dropped to zero rapidly after the bond failed. However, for the failure mode of P-FM2, after one side of the shear plane failed, the load dropped to a certain value and then showed a softening behavior due to the stress redistribution, and finally failed with two major shear cracks at both sides (see Fig. 6b). For the failure mode of specimens with the grooved interface (P-FM3), the stress history shows three load drops (see Fig. 6c). The load drop observed at Point 1 in Fig. 6c is a result of the initial

Table 4 Details of test specimens

Splitting tensile test specimen	Substrate strength (MPa)	Roughness (mm)	Moisture degree	Push-out test specimen	Substrate strength (MPa)	Roughness (mm)	Moisture degree
S-C1-R0-A-X	50.0	Smooth	ASD	P-C1-R0-A-X	50.0	Smooth	ASD
S-C1-R0-S-X		Smooth	SSD	P-C1-R0-S-X		Smooth	SSD
S-C1-R1-A-X		0.4	ASD	P-C1-R1-A-X		0.4	ASD
S-C1-R1-S-X		0.4	SSD	P-C1-R1-S-X		0.4	SSD
S-C1-R2-A-X		0.8	ASD	P-C1-R2-A-X		0.8	ASD
S-C1-R2-S-X		0.8	SSD	P-C1-R2-S-X		0.8	SSD
S-C1-R3-A-X		1.2	ASD	P-C1-R3-A-X		1.2	ASD
S-C1-R3-S-X		1.2	SSD	P-C1-R3-S-X		1.2	SSD
S-C1-R4-A-X		Grooved	ASD	P-C1-R4-A-X		Grooved	ASD
S-C1-R4-S-X		Grooved	SSD	P-C1-R4-S-X		Grooved	SSD
S-C2-R0-A-X	74.4	Smooth	ASD	P-C2-R0-A-X	74.4	Smooth	ASD
S-C2-R0-S-X		Smooth	SSD	P-C2-R0-S-X		Smooth	SSD
S-C2-R1-A-X		0.4	ASD	P-C2-R1-A-X		0.4	ASD
S-C2-R1-S-X		0.4	SSD	P-C2-R1-S-X		0.4	SSD
S-C2-R2-A-X		0.8	ASD	P-C2-R2-A-X		0.8	ASD
S-C2-R2-S-X		0.8	SSD	P-C2-R2-S-X		0.8	SSD
S-C2-R3-A-X		1.2	ASD	P-C2-R3-A-X		1.2	ASD
S-C2-R3-S-X		1.2	SSD	P-C2-R3-S-X		1.2	SSD
S-C2-R4-A-X		Grooved	ASD	P-C2-R4-A-X		Grooved	ASD
S-C2-R4-S-X		Grooved	SSD	P-C2-R4-S-X		Grooved	SSD

failure of the key joint. Subsequently, the shear stress is redistributed, leading to the disruption of all key joints and the failure of the shear plane on one side of the specimens (Point 2). From there, the shear force is transferred to the opposite side of the shear plane until both sides experience failure (Point 3).

3.2 Ultimate Strength

3.2.1 Tensile Strength

The tensile strength of the UHP-ECC to concrete interface of the splitting tensile test specimens could be calculated using the following equation:

$$\sigma_t = \frac{2N_t}{\pi A} \tag{1}$$

where σ_t is the splitting tensile strength, N_t is the applied compressive force in the splitting tensile test and A is the cross-sectional area of the interface plane. Table 5 lists the splitting tensile strengths of all the specimens. Based on the bond quality classification proposed by Sprinkel and Ozyildirim (2000), it can be observed that all specimens demonstrate excellent bond quality except for S-C2-R0-S-1 and S-C2-R0-S-2. Among the tested specimens, S-C2-R2-S-1 exhibits the highest strength, with a maximum splitting tensile strength of 5.31 MPa. This exceptional strength is attributed to the use of high-strength concrete substrates, as the observed failure mode is substrate failure. On the other hand, specimen S-C2-R0-S-2, which also utilizes high-strength concrete substrates but has a smooth interface and is subjected to the saturated surface dry (SSD) condition, exhibits the lowest splitting tensile strength among all the tested specimens, measuring at 1.05 MPa. These results indicate that factors such as surface roughness and moisture content at the interface can significantly influence the interfacial bonding strength.

3.2.2 Shear Strength

The shear strengths of the UHP-ECC to concrete interface from push-out tests are listed in Table 5. The shear strength is calculated as follows:

$$\sigma_s = \frac{N_s}{2A} \tag{2}$$

where σ_s is the shear strength, N_s is the applied shear force in the push-out test and A is the cross-sectional area of the interface plane. Despite the fact that the failure of the double-sided specimens in the push-out test occurred on one side, it is believed that prior to the generation of cracks, the shear load was evenly distributed to both shear planes as a result of meticulous alignment calibration. In Table 5, it is found that the shear strengths obtained from the push-out test are normally larger than the splitting tensile strengths with the same

Table 5 Test results

Splitting tensile test			Push-out test		
Specimens	**Failure mode**	**Splitting tensile Strength (MPa)**	**Specimens**	**Failure mode**	**Shear Strength (MPa)**
S-C1-R0-A-1	S-FM1	2.21	P-C1-R0-S-1	P-FM1	1.97
S-C1-R0-A-2	S-FM1	2.33	P-C1-R0-S-2	P-FM1	1.46
S-C1-R0-S-1	S-FM1	2.21	P-C1-R1-A-1	P-FM2	3.38
S-C1-R0-S-2	S-FM1	2.11	P-C1-R1-A-2	P-FM2	4.29
S-C1-R1-A-1	S-FM2	4.01	P-C1-R1-S-1	P-FM2	4.37
S-C1-R1-A-2	S-FM2	4.20	P-C1-R1-S-2	P-FM2	4.26
S-C1-R1-S-1	S-FM2	3.98	P-C1-R2-A-1	P-FM2	4.49
S-C1-R1-S-2	S-FM2	4.00	P-C1-R2-A-2	P-FM2	6.27
S-C1-R2-A-1	S-FM3	4.46	P-C1-R2-S-1	P-FM2	5.15
S-C1-R2-A-2	S-FM3	3.60	P-C1-R2-S-2	P-FM2	5.22
S-C1-R2-S-1	S-FM3	4.12	P-C1-R3-A-1	P-FM2	6.24
S-C1-R2-S-2	S-FM3	4.27	P-C1-R3-A-2	P-FM2	4.10
S-C1-R3-A-1	S-FM2	4.09	P-C1-R3-S-1	P-FM2	5.49
S-C1-R3-A-2	S-FM3	4.20	P-C1-R3-S-2	P-FM2	4.52
S-C1-R3-S-1	S-FM3	3.67	P-C1-R4-A-1	P-FM3	9.16
S-C1-R3-S-2	S-FM3	3.34	P-C1-R4-A-2	P-FM3	8.48
S-C1-R4-A-1	S-FM4	3.17	P-C1-R4-S-1	P-FM3	8.28
S-C1-R4-A-2	S-FM4	3.68	P-C1-R4-S-2	P-FM3	8.47
S-C1-R4-S-1	S-FM4	3.30	P-C2-R0-A-1	P-FM1	3.89
S-C1-R4-S-2	S-FM4	3.55	P-C2-R0-A-2	P-FM1	3.90
S-C2-R0-A-1	S-FM2	2.18	P-C2-R0-S-1	P-FM2	5.44
S-C2-R0-A-2	S-FM1	2.26	P-C2-R0-S-2	P-FM2	5.70
S-C2-R0-S-1	S-FM1	1.61	P-C2-R1-A-1	P-FM2	6.97
S-C2-R0-S-2	S-FM1	1.05	P-C2-R1-A-2	P-FM2	4.54
S-C2-R1-A-1	S-FM2	3.94	P-C2-R1-S-1	P-FM2	5.91
S-C2-R1-A-2	S-FM2	3.10	P-C2-R1-S-2	P-FM2	5.35
S-C2-R1-S-1	S-FM2	3.24	P-C2-R2-A-1	P-FM2	5.23
S-C2-R1-S-2	S-FM2	3.34	P-C2-R2-A-2	P-FM2	5.31
S-C2-R2-A-1	S-FM3	4.74	P-C2-R2-S-1	P-FM2	6.00
S-C2-R2-A-2	S-FM2	3.27	P-C2-R2-S-2	P-FM2	6.51
S-C2-R2-S-1	S-FM3	5.31	P-C2-R3-A-1	P-FM2	4.70
S-C2-R2-S-2	S-FM3	4.43	P-C2-R3-A-2	P-FM2	5.89
S-C2-R3-A-1	S-FM3	2.90	P-C2-R3-S-1	P-FM2	4.50
S-C2-R3-A-2	S-FM3	2.90	P-C2-R3-S-2	P-FM2	5.72
S-C2-R3-S-1	S-FM3	4.07	P-C2-R4-A-1	P-FM3	8.13
S-C2-R3-S-2	S-FM2	4.21	P-C2-R4-A-2	P-FM3	8.44
S-C2-R4-A-2	S-FM4	3.14	P-C2-R4-S-1	P-FM3	9.98
S-C2-R4-S-1	S-FM4	3.00	P-C2-R4-S-2	P-FM3	8.89
S-C2-R4-S-2	S-FM4	3.63			
S-C2-R4-A-2	S-FM4	3.43			

interface parameters, especially for the specimens with grooved interface. The presence of key joints in the interface greatly enhanced the shear adhesion properties of the UHP-ECC to concrete interface. Among all the specimens, the maximum shear strength is 9.98 MPa which was achieved in specimen P-C2-R4-S-1, a specimen with high strength concrete substrate, and grooved interface under SSD condition. The minimum shear strength occurred in specimen P-C1-R0-S-1 with normal strength substrates and smooth surface under ASD condition.

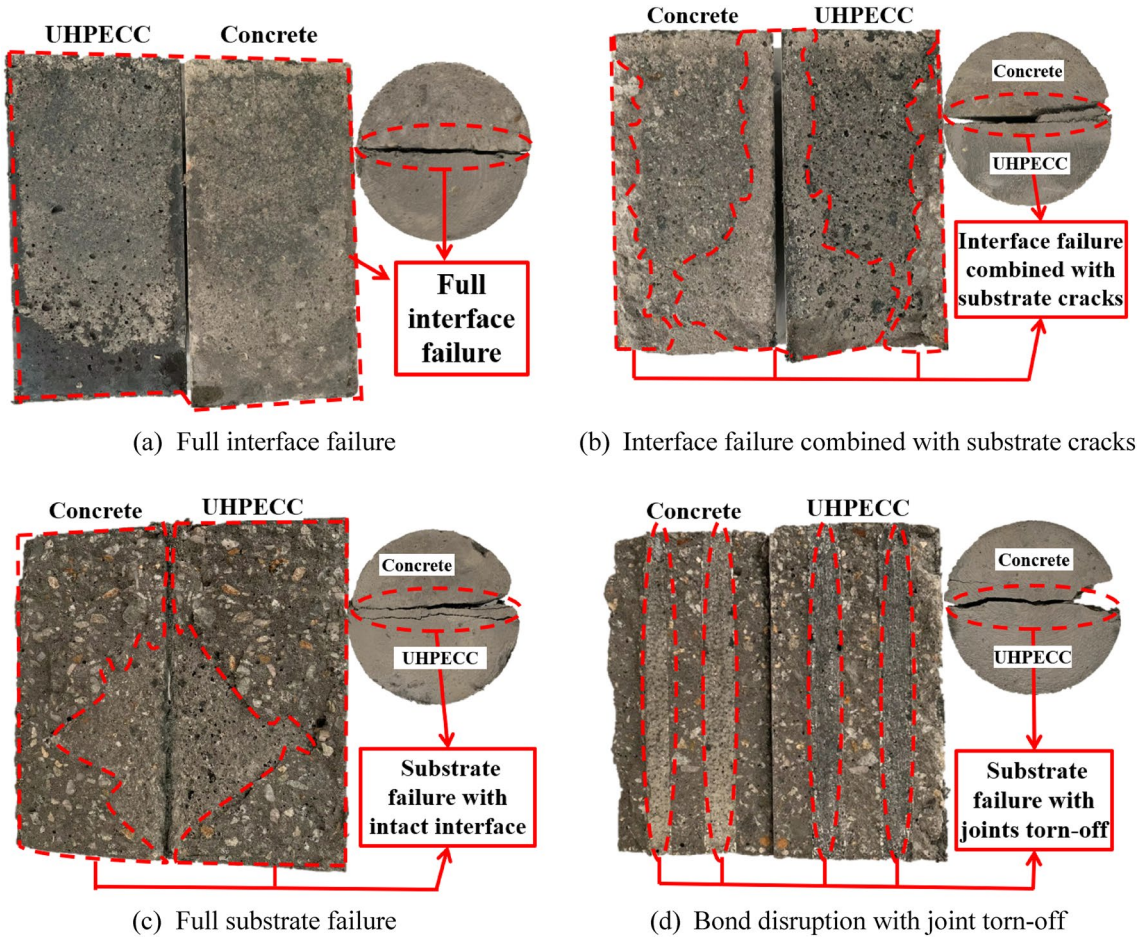

Fig. 4 Failure modes of splitting tensile tests

3.3 Influence of the Studied Parameters

3.3.1 Strength of Concrete Substrate

Two types of concrete substrates were utilized in the study: normal strength concrete with a cylinder strength of 50.0 MPa and high strength concrete with a cylinder strength of 74.4 MPa. Fig. 7 presents a comparison between specimens featuring different substrate strengths. The relationship between the increase in differential compressive strength and bond strength shows a positive correlation for the specimens with interface roughness levels of R2 and R3 in the splitting tensile tests (see Fig. 7a) and specimens with all levels of roughness in the push-out tests (see Fig. 7b). The increase in the grade of concrete improves the tensile strength of the substrate, thus for the specimens that failed with cracking of the substrate, the ultimate strength could be increased. It could be found in Fig. 7, that the ultimate strength of C2 substrates is higher in those specimen pairs with failure mode of full substrates failure. The ultimate splitting tensile strengths of specimen series S-C2-R0-S-X and S-C2-R1-S-X are smaller than their counterparts with lower concrete strength because full interface failures occurred in which the tensile strength of substrates no longer dominates the tensile capacity. In Fig. 7b, it is evident that the shear strength of the interface tends to rise with higher strength of the substrate concrete. Notably, the specimen group P-C1-R0-S failed with full interface shear failure, but an increase in substrate strength led to a shift in the failure mode from full interface failure to concrete substrate shear failure, indicating that the increase in substrate strength may impact the shear capacity of the interface. This observation differs from the findings of the splitting tensile test. However, due to the limited number of test data, the reason for such influence remains uncertain, and the failure mechanism warrants further exploration through additional test data and microstructural analysis.

3.3.2 Moisture Degree of Substrate Surface

The influence of air surface dry condition and saturated surface dry condition on interface bond behavior is

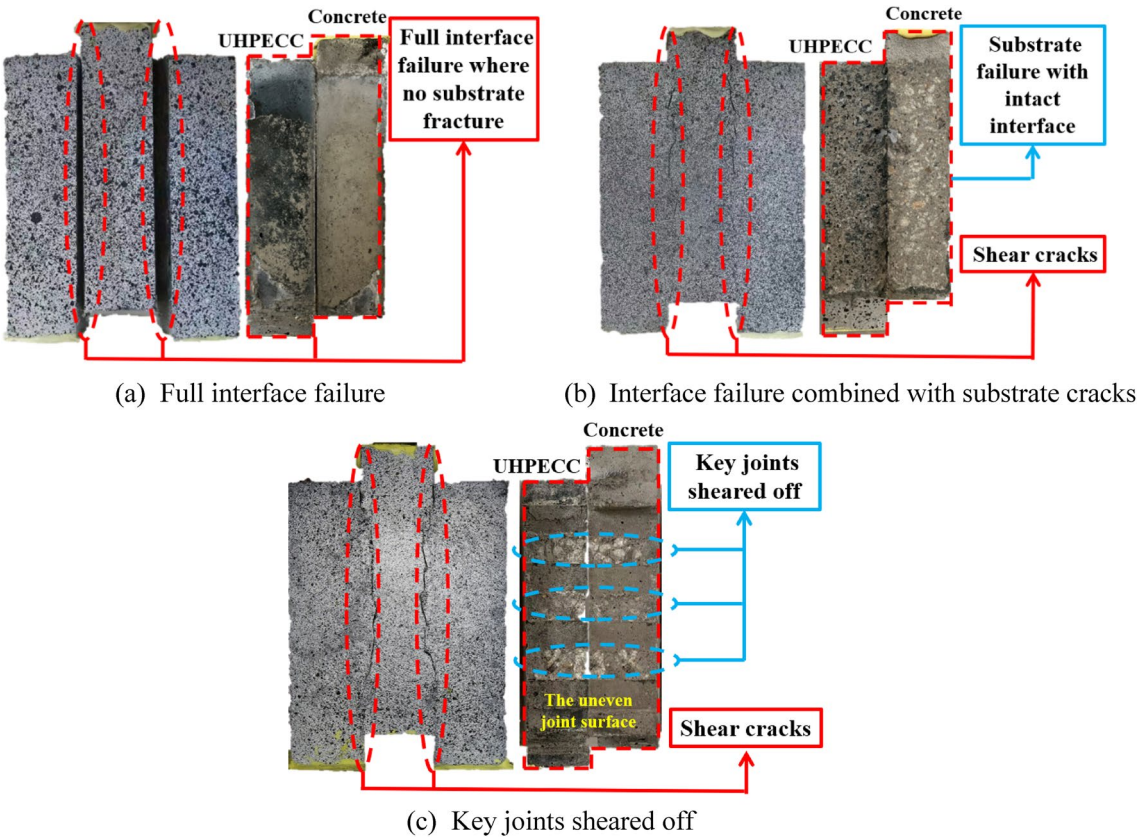

Fig. 5 Failure modes of Push-out tests

investigated in the current study. Fig. 8 shows the comparison of splitting tensile strength and shear strength of the specimens with air surface dry condition and saturated surface dry condition. As the water/binder ratio in UHP-ECC is very low, during the casting of UHP-ECC, the strong hydrophilicity of the NSC substrate enables the transfer of water to the UHPC overlay. This transfer may result in a decrease in the water content of the UHPC, and could potentially lead to incomplete hydration reactions. As a result, this incomplete hydration may compromise the bond strength at the UHP-ECC-to-NSC interface. Therefore, in the specimen with substrates under ASD condition, the UHP-ECC overlayer may be weaker than that with SSD condition. Based on Fig. 8, it was observed that the moisture condition of the substrate surface has minimal effect on the splitting tensile strength and shear strength. This can be attributed to the fact that the tensile and shear strength of UHP-ECC significantly surpasses that of the substrates. Consequently, the impact of the moisture condition on the strength of the overlayers becomes relatively minor in relation to the overall bonding strength.

3.3.3 Roughness

Surface roughness is a key parameter to the bonding strength of concrete. The averaged splitting tensile strengths and shear strengths with different roughness are compared in Fig. 9. Based on the observations from Fig. 9, it could be found when the surface roughness switched from smooth to rough surface with macrotexture depths of 0.4 mm (R1), the splitting tensile strength and shear strength increased by 83% and 51% respectively. However, when the surface macrotexture depth increases from 0.4 to 0.8 mm, the splitting tensile strength and shear strength only increased by 15% and 13% while when the number increases from 0.8 to 1.2 mm, the strengths show small degradations with 14% and 7%. The result shows that the increasing surface macrotexture depth is not always beneficial to the bonding strength between concrete and UHP-ECC. The interpretation could be that the specimens with roughness levels higher than R2 failed with full substrate disruption, and the interface roughness may have a minor influence on the tensile or shear capacity of the specimens due to change in the bonding mechanism. Another observation is that the grooving of the interface is highly beneficial in improving the shear capacity of the specimens where the

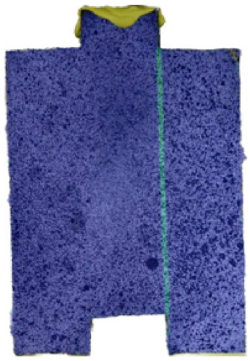

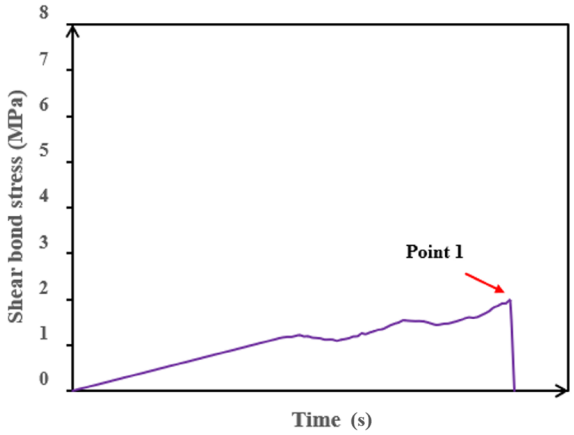

(a) Specimen P-C1-R0-S1 with failure mode P-FM1

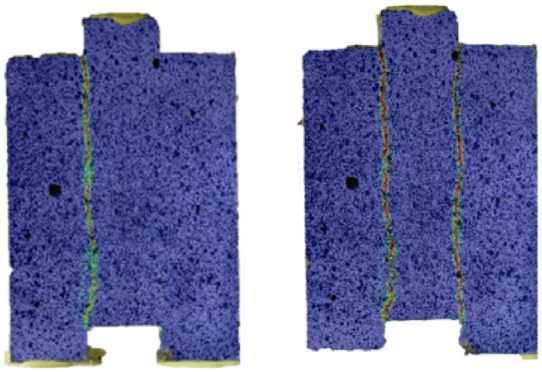

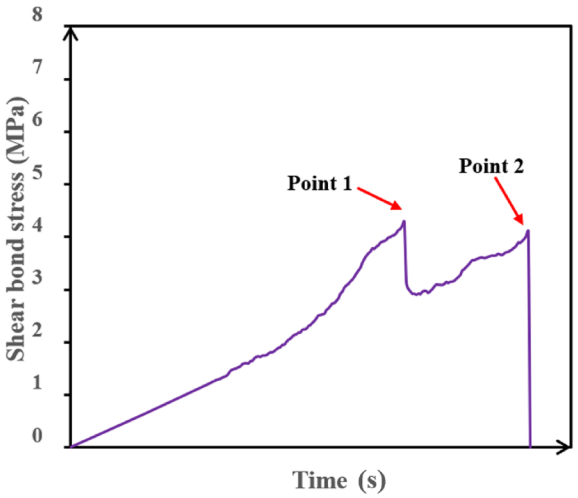

(b) Specimen P-C1-R1-A2 with failure mode P-FM2

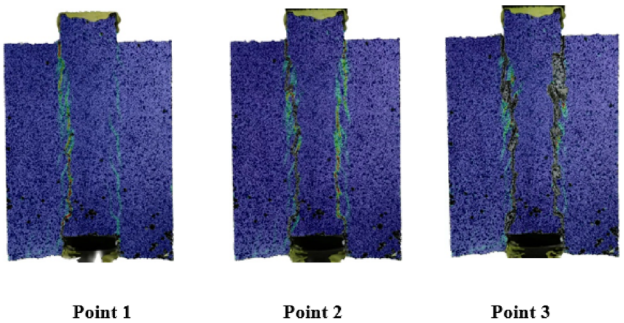

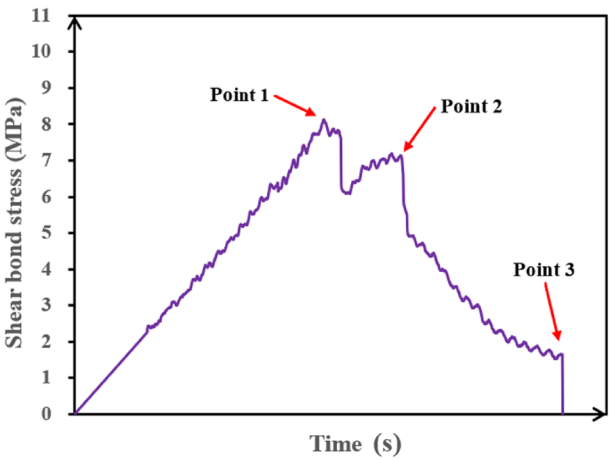

(c) Specimen P-C2-R4-A2 with failure mode P-FM3

Fig. 6 Strain distribution and stress history of specimens with different failure modes

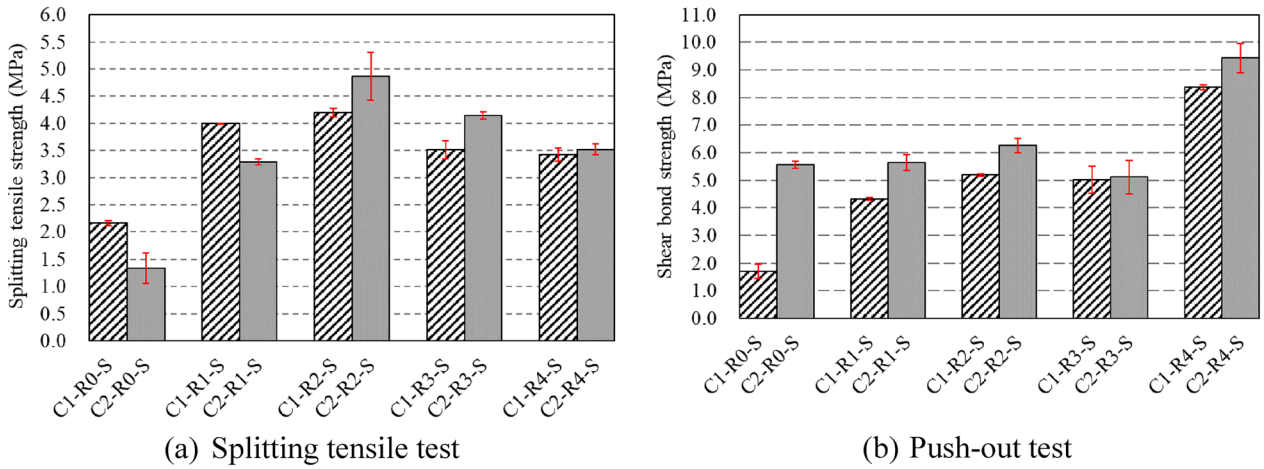

Fig. 7 Comparison between specimens with different substrate strengths

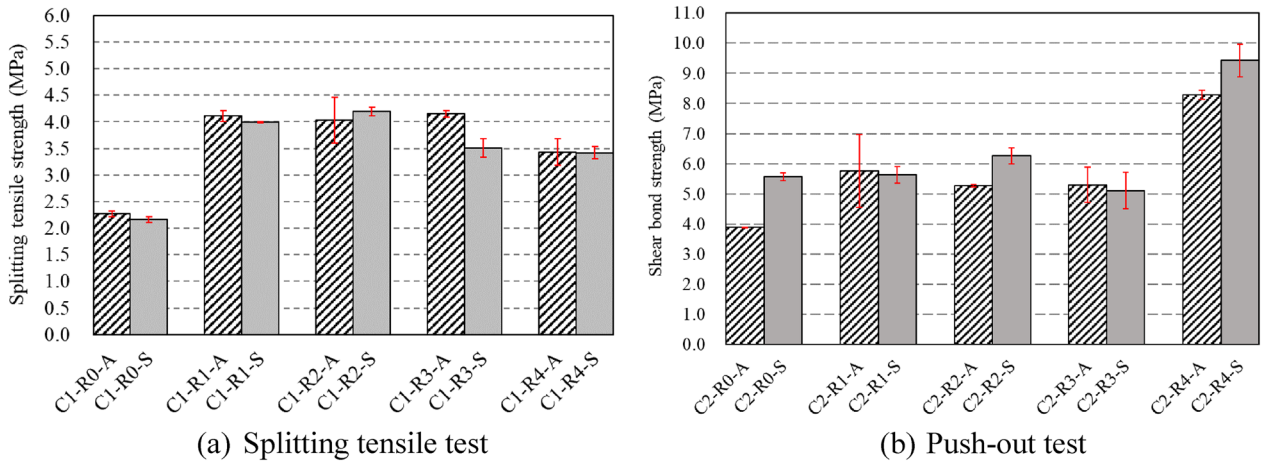

Fig. 8 Comparison between specimens with different moisture condition

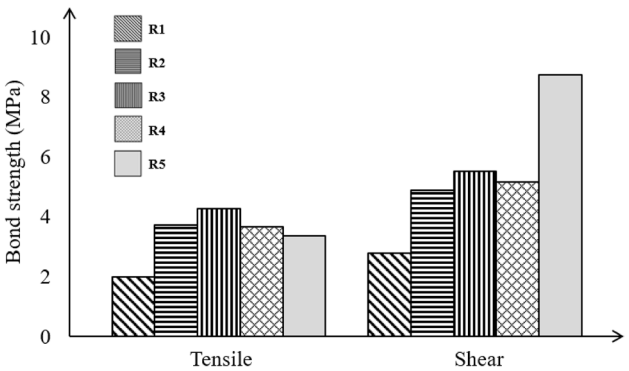

Fig. 9 Comparison between specimens with different surface roughness

averaged shear strength is increased by 67% compared with the strength from specimens with a macrotexture depth of 1.2 mm (i.e., R3). However, this observation is not found in the splitting tensile tests, the specimens with grooved interface have a similar tensile capacity with the specimens with a roughness level of R3.

4 Prediction Models

The experimental observation indicated that the splitting tensile strength and shear strength of the UHP-ECC to concrete interface are correlated to the interface roughness and substrate strength. In this section, prediction models of tensile strength and shear

strength were proposed for the UHP-ECC to concrete interface based on the 78 test data presented in this paper.

The base equation of the models is adopted from Wang et al. (2018). The expression is shown as follows:

$$f = a(t_1 S + t_2)(t_3 R + t_4) \tag{3}$$

where f is tensile or shear strength of the specimen, a is the rate constant, S is the substrate strength, and R is the macrotexture depth of the substrate surface and t_1, t_2, t_3, t_4, are the coefficients to be determined based on the test results. After the regression analysis based on the current experimental data, the prediction models for the tensile strength and shear strength of the UHP-ECC to concrete interface were given as follows:

$$f_s = 0.6(0.36S + 2)(0.7R + 1.4) \tag{4}$$

$$f_p = 1.45(0.002S + 1.2)(1.95R + 0.95) \tag{5}$$

where f_s and f_p are the tensile strength and shear strength of the UHP-ECC to concrete interface. Fig. 10 shows the performance of the prediction models. It could be found that the model could reasonably capture the experimental results from the splitting tensile tests and push-out tests.

5 Conclusions

The findings of an experimental investigation on the tensile and shear behavior of the interface between UHP-ECC and concrete have been presented in this paper. The focusing parameters including the substrate concrete strength, the surface moisture condition, and the surface roughness on the failure mode and ultimate strength of the specimens have been comprehensively explored. Furthermore, based on the test results, prediction models have been proposed to accurately predict the splitting tensile strength and shear strength of the UHP-ECC to concrete interface. The study yielded several significant conclusions as below.

1. The splitting tensile tests revealed four distinct failure modes. Specimens with a smooth substrate surface, without any surface treatment, predominantly experienced full interface debonding. As the surface roughness increased, the failure mode transitioned from full interface failure to a combination of interface failure and substrate cracks, and ultimately full substrate failure with an intact interface was achieved when the roughness of the interface was large. The specimens with a grooved surface exhibited torn-off key joints as the primary failure mode. In the push-out tests, specimens with a smooth interface predominantly failed due to interface debonding. On the other hand, specimens with surface treatment exhibited full substrate shear failure. Similarly, specimens with a grooved surface experienced sheared-off key joints during the push-out tests.

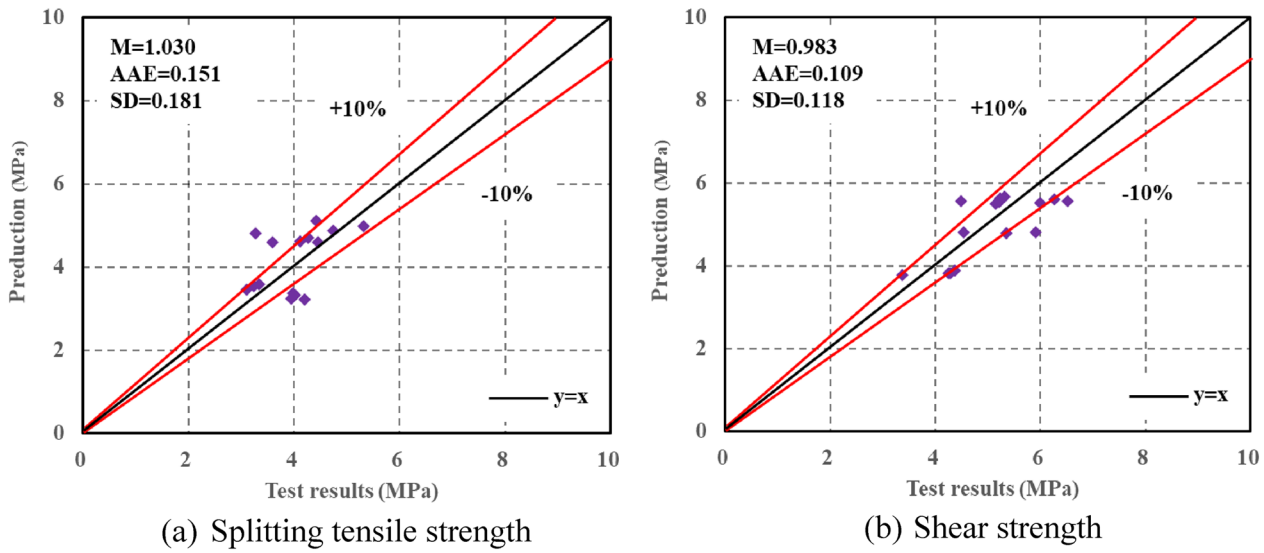

(a) Splitting tensile strength (b) Shear strength

Fig. 10 Assessment of proposed strength models

2. A direct correlation was observed between the ultimate strength and the substrate concrete strength in specimens that exhibited full substrate failure in both the splitting tensile tests and the push-out tests. However, the influence of substrate strength was found to be relatively minor in the specimens that experienced interface debonding or interface debonding combined with substrate cracks.
3. The test results revealed that the moisture condition at the substrate surface had a negligible impact. This can be attributed to the superior tensile and shear strength of UHP-ECC, which significantly surpasses that of the substrates. As a result, the strength of the overlayers becomes less significant in relation to the overall bonding strength.
4. The roughness of the substrate surface plays a crucial role in the interfacial bonding behavior between UHP-ECC and concrete. A substantial improvement in tensile capacity (up to 83%) was observed when the smooth interface was chiseled to macrotexture depths of 0.4 mm. However, the enhancement margin diminishes as the macrotexture depth increases, and a decrease in strength was noted when the macrotexture depths increased from 0.8 mm to 1.2 mm. The grooving treatment is highly effective in improving the shear strength of the interface, but it has a lesser impact on enhancing the tensile strength.
5. Predictive models for the tensile strength and shear strength of the UHP-ECC to concrete interface were developed, providing a high level of accuracy in capturing the experimental results.

Acknowledgements
The authors acknowledge the financial support received from the National Natural Science Foundation of China (No. 52208317), and the Natural Science Foundation of Guangdong Province (Nos. 2021B1515020029, 2021A0505060008, and 2022A1515240008).

Author contributions
Jun-Jie Zeng: Conceptualization, Funding acquisition, Supervision, Methodology, Writing—review and editing; Xin-Chao Lin: Methodology, Investigation, Data curation; Sheng-Zhao Feng: Methodology, Investigation, Data curation; Jiong-Yi Zhu: Conceptualization, Data curation, Writing—original draft; Yan Zhuge: Writing—review and editing; Yihang Yan: Writing—review and editing.

Funding
This research was supported by the National Natural Science Foundation of China (No. 52208317), and the Natural Science Foundation of Guangdong Province (Nos. 2021B1515020029, 2021A0505060008, and 2022A1515240008).

Availability of data and materials
All data generated or analyzed during this study are included in this published article.

Declarations

Ethics approval and consent to participate
Not applicable.

Consent for publication
Not applicable.

Competing interests
The authors declare that they have no competing interests.

Received: 21 September 2023 Accepted: 21 March 2024
Published online: 06 August 2024

References

ASTM. (2014). Standard test method for static modulus of elasticity and Poisson's ratio of concrete in compression. In *ASTM C469–02* (Vol. C469–02). West Conshohocken: ASTM.

ASTM. (2019). Standard test method for measuring pavement macrotexture depth using a volumetric technique. In *ASTM E965–96* (Vol. E965–96). West Conshohocken: ASTM.

Bentz, D. P., De la Varga, I., Muñoz, J. F., Spragg, R. P., Graybeal, B. A., Hussey, D. S., Jacobson, D. L., Jones, S. Z., & LaManna, J. M. (2018). Influence of substrate moisture state and roughness on interface microstructure and bond strength: Slant shear vs. pull-off testing. *Cement and Concrete Composites, 87*, 63–72. https://doi.org/10.1016/j.cemconcomp.2017.12.005

Deng, M., Dong, Z., & Ma, P. (2019). Cyclic loading tests of flexural-failure dominant URM walls strengthened with engineered cementitious composite. *Engineering Structures, 194*, 173–182. https://doi.org/10.1016/j.engstruct.2019.05.073

Diab, A. M., Abd Elmoaty, A. E. M., & Tag Eldin, M. R. (2017). Slant shear bond strength between self compacting concrete and old concrete. *Construction and Building Materials, 130*, 73–82. https://doi.org/10.1016/j.conbuildmat.2016.11.023

Ding, Y., Yu, J.-T., Yu, K.-Q., & Xu, S.-L. (2018). Basic mechanical properties of ultra-high ductility cementitious composites: From 40 MPa to 120 MPa. *Composite Structures, 185*, 634–645. https://doi.org/10.1016/j.compstruct.2017.11.034

El Afandi, M., Yehia, S., Landolsi, T., Qaddoumi, N., & Elchalakani, M. (2023). Concrete-to-concrete bond strength: A review. *Construction and Building Materials, 363*, 129820. https://doi.org/10.1016/j.conbuildmat.2022.129820

Farzad, M., Shafieifar, M., & Azizinamini, A. (2019). Experimental and numerical study on bond strength between conventional concrete and Ultra High-Performance Concrete (UHPC). *Engineering Structures, 186*, 297–305. https://doi.org/10.1016/j.engstruct.2019.02.030

Ju, Y., Shen, T., & Wang, D. (2020). Bonding behavior between reactive powder concrete and normal strength concrete. *Construction and Building Materials, 242*, 118024. https://doi.org/10.1016/j.conbuildmat.2020.118024

Júlio, E. N. B. S., Branco, F. A. B., & Silva, Vt. D. (2004). Concrete-to-concrete bond strength Influence of the roughness of the substrate surface. *Construction and Building Materials, 18*(9), 675–681. https://doi.org/10.1016/j.conbuildmat.2004.04.023

Li, V. C. (2003). On Engineered Cementitious Composites (ECC) a review of the material and its applications. *Journal of Advanced Concrete Technology, 1*(3), 215–230. https://doi.org/10.3151/jact.1.215

Li, L.-Z., Bai, Y., Yu, K.-Q., Yu, J.-T., & Lu, Z.-D. (2019). Reinforced high-strength engineered cementitious composite (ECC) columns under eccentric compression: Experiment and theoretical model. *Engineering Structures, 198*, 109541. https://doi.org/10.1016/j.engstruct.2019.109541

Li, S., Chen, X., Liu, Z., Lu, Y., & Wang, H. (2023). Axial behavior of pre-damaged RC columns strengthened with CFRP textile grid-reinforced ECC matrix composites. *Journal of Building Engineering, 73*, 106813. https://doi.org/10.1016/j.jobe.2023.106813

Li, V. C., Wang, S., & Wu, C. (2001). Tensile strain-hardening behavior of polyvinyl alcohol engineered cementitious composite (PVA-ECC). *Materials Journal, 98*(6), 483–492.

Li, Z.-Q., Hou, W., & Lin, G. (2021). Flexural strengthening of RC beams with BFRP or high strength steel bar–reinforced ECC matrix. *Construction and Building Materials, 303*, 124404. https://doi.org/10.1016/j.conbuildmat.2021.124404

Lin, Y.-W., Wotherspoon, L., Scott, A., & Ingham, J. M. (2014). In-plane strengthening of clay brick unreinforced masonry wallettes using ECC shotcrete. *Engineering Structures, 66*, 57–65. https://doi.org/10.1016/j.engstruct.2014.01.043

Lin, G., Zeng, J., Li, J., Chen, G.M. (2024) Chord axial compressive behavior of hybrid FRP-concrete-steel double-skin tubularmember T-joints. Thin-Walled Structures, *196*, 111535.

Luo, Q., Qin, T., Chen, Z., Pang, B., Qu, J., & Gao, Z. (2023). The influence of moisture and epoxy bonding agents on interfacial behavior between normal concrete substrate and ultrahigh performance concrete as a repair material: Experimental and molecular dynamics study. *Construction and Building Materials, 372*, 130779. https://doi.org/10.1016/j.conbuildmat.2023.130779

Pan, B., Liu, F., Zhuge, Y., Zeng, J.-J., & Liao, J. (2022). ECCs/UHPFRCCs with and without FRP reinforcement for structural strengthening/repairing: A state-of-the-art review. *Construction and Building Materials, 316*, 125824. https://doi.org/10.1016/j.conbuildmat.2021.125824

Qasim, M., Lee, C. K., & Zhang, Y. X. (2022). An experimental study on interfacial bond strength between hybrid engineered cementitious composite and concrete. *Construction and Building Materials, 356*, 129299. https://doi.org/10.1016/j.conbuildmat.2022.129299

Santos, P. M. D., Júlio, E. N. B. S., & Silva, Vt. D. (2007). Correlation between concrete-to-concrete bond strength and the roughness of the substrate surface. *Construction and Building Materials, 21*(8), 1688–1695. https://doi.org/10.1016/j.conbuildmat.2006.05.044

Semendary, A. A., & Svecova, D. (2020). Factors affecting bond between precast concrete and cast in place ultra high performance concrete (UHPC). *Engineering Structures, 216*, 110746. https://doi.org/10.1016/j.engstruct.2020.110746

Sprinkel, M. M. O. C. (2000). *Evaluation of high performance concrete overlays placed on Route 60 over Lynnhaven Inlet in Virginia* (VTRC-01-R1). V. T. R. Council. https://rosap.ntl.bts.gov/view/dot/15370

Tian, J., Wu, X., Tan, X., Wang, W.-W., Hu, S., Du, Y., Yuan, J., Huang, W., & Huang, X. (2022). Experimental study and analysis model of flexural synergistic effect of reinforced concrete beams strengthened with ECC. *Construction and Building Materials, 352*, 128987. https://doi.org/10.1016/j.conbuildmat.2022.128987

Tian, J., Wu, X., Zheng, Y., Hu, S., Du, Y., Wang, W., Sun, C., & Zhang, L. (2019). Investigation of interface shear properties and mechanical model between ECC and concrete. *Construction and Building Materials, 223*, 12–27. https://doi.org/10.1016/j.conbuildmat.2019.06.188

Wang, B., Li, Q., Liu, F., Wang, J., & Xu, S. (2018). Shear bond assessment of UHTCC repair using push-out test. *Construction and Building Materials, 164*, 206–216. https://doi.org/10.1016/j.conbuildmat.2017.12.148

Wang, G., Wei, Y., Chen, S., Zhao, K., & Zhou, Z. (2023a). Bond performance between surface-modified bamboo bars and concrete under pull-out loading. *Journal of Building Engineering, 79*, 107920. https://doi.org/10.1016/j.jobe.2023.107920

Wang, G., Wei, Y., Shen, C., Huang, Z., & Zheng, K. (2023b). Compression performance of FRP-steel composite tube-confined ultrahigh-performance concrete (UHPC) columns. *Thin-Walled Structures, 192*, 111152. https://doi.org/10.1016/j.tws.2023.111152

Yang, X., Gao, W.-Y., Dai, J.-G., Lu, Z.-D., & Yu, K.-Q. (2018). Flexural strengthening of RC beams with CFRP grid-reinforced ECC matrix. *Composite Structures, 189*, 9–26. https://doi.org/10.1016/j.compstruct.2018.01.048

Yan, Z.T., Zeng, J.J., Zhuge, Y., Liao, J.J., Zhou, J.K., Ma, G.W. (2024). Compressive behavior of FRP-confined 3D printed ultra-highperformance concrete cylinders, J. Build. Eng. *81*, 108304.

Ye, M., Li, L., Pei, B., Yoo, D.-Y., & Li, H. (2023). Shear behavior of externally prestressed ultra-high-performance concrete (UHPC) T-beams without stirrups. *Engineering Structures, 288*, 116217. https://doi.org/10.1016/j.engstruct.2023.116217

Yoo, D.-Y., & Banthia, N. (2016). Mechanical properties of ultra-high-performance fiber-reinforced concrete: A review. *Cement and Concrete Composites, 73*, 267–280. https://doi.org/10.1016/j.cemconcomp.2016.08.001

Yu, J., Dong, Z., Yu, J., Liu, F., Ye, J., & Dong, F. (2022). Dynamic response of masonry walls strengthened with engineered cementitious composites under simulated debris flow. *Journal of the Structural Engineering. American Society of Civil Engineers, 148*(9), 04022113. https://doi.org/10.1061/(ASCE)ST.1943-541X.0003432

Yu, K.-Q., Lu, Z.-D., Dai, J.-G., & Shah, S. P. (2020). Direct tensile properties and stress-strain model of UHP-ECC. *J Mater Civil Mater, 32*(1), 04019334. https://doi.org/10.1061/(ASCE)MT.1943-5533.0002975

Yu, K.-Q., Yu, J.-T., Dai, J.-G., Lu, Z.-D., & Shah, S. P. (2018). Development of ultra-high performance engineered cementitious composites using polyethylene (PE) fibers. *Construction and Building Materials, 158*, 217–227. https://doi.org/10.1016/j.conbuildmat.2017.10.040

Zanotti, C., Banthia, N., & Plizzari, G. (2014). A study of some factors affecting bond in cementitious fiber reinforced repairs. *Cement and Concrete Research, 63*, 117–126. https://doi.org/10.1016/j.cemconres.2014.05.008

Zanotti, C., Borges, P. H. R., Bhutta, A., & Banthia, N. (2017). Bond strength between concrete substrate and metakaolin geopolymer repair mortar: Effect of curing regime and PVA fiber reinforcement. *Cement and Concrete Composites, 80*, 307–316. https://doi.org/10.1016/j.cemconcomp.2016.12.014

Zeng, J.-J., Liang, Q.-J., Cai, W.-J., Liao, J., Zhou, J.-K., Zhu, J.-Y., & Zhang, L. (2023). Strengthening RC square columns with UHP-ECC section curvilinearization and FRP confinement: Concept and axial compression tests. *Engineering Structures, 280*, 115666. https://doi.org/10.1016/j.engstruct.2023.115666

Zhang, C., Wu, L., Yu, Z., Gu, J., Ukrainczyk, N., & Cai, J. (2023). Effect of roughness on the bond behavior between ultrahigh-performance engineered cementitious composites and old concrete. *J Mater Civil Eng, 35*(8), 04023268. https://doi.org/10.1061/JMCEE7.MTENG-15735

Zhang, R., Meng, Q., Shui, Q., He, W., Chen, K., Liang, M., & Sun, Z. (2019). Cyclic response of RC composite bridge columns with precast PP-ECC jackets in the region of plastic hinges. *Composite Structures, 221*, 110844.

Zhang, Y., Deng, M., Li, T., & Dong, Z. (2021). Strengthening of flexure-dominate RC columns with ECC jackets: Experiment and analysis. *Engineering Structures, 231*, 111809. https://doi.org/10.1016/j.engstruct.2020.111809

Zhang, Y., Zhu, P., Liao, Z., & Wang, L. (2020). Interfacial bond properties between normal strength concrete substrate and ultra-high performance concrete as a repair material. *Construction and Building Materials, 235*, 117431. https://doi.org/10.1016/j.conbuildmat.2019.117431

Zhao, Z., Wei, Y., Wang, G., Zhang, Y., & Lin, Y. (2023). Axial compression performance of square UHPC-filled stainless-steel tubular columns. *Construction and Building Materials, 408*, 133622. https://doi.org/10.1016/j.conbuildmat.2023.133622

Zeng, J., Zeng, W.B., Zhuge, Y., Zhou, J.K., Quach, W.M., Feng, R. (2024). Behavior and modeling of FRP grid-reinforced ultra-highperformanceconcrete under uniaxial tension, Structural Concrete. SUCO202300576.https://doi.org/10.1002/suco.202300576

Publisher's Note

Jun-Jie Zeng is now a Senior lecturer at UniSA STEM, University of South Australia.

Xin-Chao Lin is now a master degree student in Department of Civil Engineering at Guangdong University of Technology.

Sheng-Zhao Feng is now a master degree student in Department of Civil Engineering at Guangdong University of Technology.

Jiong-Yi Zhu is now a lecturer in Department of Civil Engineering, School of Mechanics and Engineering Science at Shanghai University.

Yan Zhuge is now a professor at University of South Australia.

Yihang Yan is now an engineer at Shanghai Urban Construction and Design Research Institute (Group) Co.